Effective radii of deuteron-induced reactions

Shintaro Hashimoto,[1,*] Masanobu Yahiro,[2] Kazuyuki Ogata,[2] Kosho Minomo,[2] and Satoshi Chiba[1]
[1]*Advanced Science Research Center, Japan Atomic Energy Agency, Ibaraki 319-1195, Japan*
[2]*Department of Physics, Kyushu University, Fukuoka 812-8581, Japan*
(Received 31 March 2011; published 27 May 2011)

The continuum-discretized coupled-channels method (CDCC) for exclusive reactions and the eikonal reaction theory (ERT) as an extension of CDCC to inclusive reactions are applied to deuteron-induced reactions. The CDCC result reproduces experimental data on the reaction cross section for $d + {}^{58}$Ni scattering at 200 MeV/nucleon, and ERT provides data on the neutron-stripping cross section for inclusive ^{7}Li(d,n) reaction at 40 MeV. For deuteron-induced reactions at 200 MeV/nucleon, target-dependence of the reaction, elastic-breakup, nucleon-stripping, nucleon-removal, and complete- and incomplete-fusion cross sections is clearly explained by simple formulas. Accuracy of the Glauber model is also investigated.

DOI: 10.1103/PhysRevC.83.054617 PACS number(s): 24.10.Eq, 25.45.Hi, 25.60.Gc, 25.60.Pj

I. INTRODUCTION

Understanding of the fusion reaction mechanism is one of the most important and challenging subjects in nuclear physics. The fusion reaction consists of complete and incomplete fusion processes. In the complete fusion process, all of the projectile is absorbed by the target nucleus. In the incomplete fusion process, meanwhile, a part of the projectile is absorbed, while other parts of the projectile are emitted. The complete fusion process at low-incident energies is essential to understand the production of superheavy nuclei. The incomplete fusion process in the scattering of unstable nuclei at intermediate energies is important to extract information on the projectile from the scattering. Actually, the nucleon-removal reaction widely used for the spectroscopy of unstable nuclei [1] is composed of the nucleon-stripping reaction as a consequence of the incomplete fusion process and the elastic-breakup reaction as a result of the direct-reaction process. Furthermore, the proton-stripping process in inclusive ^{7}Li(d,n) reaction at incident energies up to 50 MeV attracts the interest of not only nuclear physicists but also nuclear engineers, because emitted neutrons through the process are planned to be used in the International Fusion Materials Irradiation Facility (IFMIF) [2]. Accurate evaluation of the proton-stripping cross section is highly required.

The theoretical tool of analyzing the incomplete fusion process at intermediate energies is the Glauber model [3]. The theoretical foundation of the model is investigated in Ref. [4]. The Glauber model is based on the eikonal and the adiabatic approximation; the latter is known to make the elastic-breakup and removal cross sections diverge when the Coulomb interaction is included; see, for example, Ref. [5]. The Glauber model has thus been applied only for lighter targets in which the Coulomb interaction is negligible; see, for example, Refs. [1,6–16]. Very recently, inclusive ^{7}Li(d,n) reaction at 40 MeV [17] was analyzed by the hybrid calculation [18] in which the elastic-breakup component is evaluated by the continuum-discretized coupled-channels method (CDCC) [19,20] and the proton stripping component is by the Glauber model. The analysis was successful in reproducing the data [17], even if the Coulomb interaction is neglected in the Glauber-model calculation. Such a hybrid calculation should be justified by more accurate reaction theories.

CDCC is an accurate method for treating exclusive reactions such as elastic scattering and elastic-breakup reactions. The theoretical foundation of CDCC is shown in Refs. [21–23]. CDCC succeeded in reproducing data on the scattering of stable and unstable projectiles [19,20,24–37]. Very recently, CDCC was extended to inclusive reactions such as nucleon-stripping reactions [38]. This method is referred to as the eikonal reaction theory (ERT). In ERT, the adiabatic approximation is not made for the Coulomb interaction, so that the elastic-breakup and the nucleon removal reaction never diverge. ERT is thus applicable for both light and heavy targets. ERT assumes the eikonal approximation to be good. The formulation starts with the eikonal approximation, but non-eikonal corrections are made by calculating fusion cross sections with CDCC. This is essential progress in the theory on fusion reactions.

Extensive measurements of total-reaction and nucleon-removal cross sections are now being made for the scattering of unstable nuclei at intermediate energies, say 100–300 MeV/nucleon, in MSU, RIKEN, and GSI. Accurate understanding of the fusion-reaction mechanism is thus highly required at intermediate energies. In this paper, we mainly consider deuteron-induced reactions at 200 MeV/nucleon as a typical case and analyze integrated cross sections of the reactions with CDCC and ERT. Deuteron is as fragile as an unstable nuclei and, furthermore, it has no ambiguity of structure. In this sense, deuteron is the most suitable projectile to understand the fusion-reaction mechanism. We will show that CDCC reproduces experimental data on the reaction cross section for $d + {}^{58}$Ni scattering at 200 MeV/nucleon, and ERT provides data on the neutron-stripping cross section for inclusive ^{7}Li(d,n) reaction at 40 MeV. Target-mass-number (A) dependence of the reaction, elastic-breakup, nucleon-removal, nucleon-stripping, and incomplete- and complete-fusion cross sections for deuteron-induced reactions at 200 MeV/nucleon

*hashimoto.shintaro@jaea.go.jp

 ©2011 American Physical Society

is clearly explained with simple formulas. Accuracy of the Glauber model will be investigated.

ERT is recapitulated in Sec. II. Numerical results of CDCC and ERT are presented in Sec. III. Section IV is devoted to summary.

II. EIKONAL REACTION THEORY

A. Three-body model

Deuteron (d) is the system in which proton (p) and neutron (n) are weakly bound. It is thus natural to assume that scattering of d from target T is well described by the $p+n+$T three-body model. Actually, the model is successful in reproducing the experimental data on elastic scattering and breakup reactions of d [19,20]. The model Hamiltonian is

$$H = -\frac{\hbar^2}{2\mu}\nabla_R^2 + U(r_p, r_n) + h \tag{1}$$

with

$$U(r_p, r_n) = U_p^{(\mathrm{N})}(r_p) + U_p^{(\mathrm{C})}(r_p) + U_n^{(\mathrm{N})}(r_n), \tag{2}$$

where $h = T_r + V(\boldsymbol{r})$ denotes the intrinsic Hamiltonian of d that consists of the kinetic-energy operator T_r and the interaction V. Furthermore, μ is the reduced mass between d and T, $U_p^{(\mathrm{N})}$ [$U_n^{(\mathrm{N})}$] is the nuclear part of the proton (neutron) optical potential and $U_p^{(\mathrm{C})}$ is the Coulomb interaction between p and T. The three-dimensional vector $\boldsymbol{R} = (\boldsymbol{b}, Z)$ stands for the coordinate between d and T, while $\boldsymbol{r}$ is the coordinate between p and n. The vector $\boldsymbol{r}_x = (\boldsymbol{b}_x, z_x)$ for $x = p$ or n is the coordinate between x and T. The total wave function $\Psi(\boldsymbol{R}, \boldsymbol{r})$ of the three-body system is then obtained by solving the three-body Schrödinger equation

$$[H - E]\Psi(\boldsymbol{R}, \boldsymbol{r}) = 0. \tag{3}$$

In the three-body model, transitions of the incident flux to the inelastic (target-excitation) channels are expressed by the imaginary parts of $U_p^{(\mathrm{N})}$ and $U_n^{(\mathrm{N})}$. The imaginary part of $U_p^{(\mathrm{N})}$ denotes the absorption of p by T, while the imaginary part of $U_n^{(\mathrm{N})}$ corresponds to the absorption of n by T. Therefore, the three-body model implicitly assumes that p and n are absorbed independently.

B. Separation of S matrix

We consider d scattering at intermediate energies, say 200 MeV/nucleon. Since the eikonal approximation is considered to be good for the scattering, the S-matrix elements and several types of cross sections are described by ERT. Accuracy of the eikonal approximation is investigated later. In this subsection, we recapitulate ERT for deuteron scattering. In the eikonal approximation, the three-body wave function Ψ is assumed to be

$$\Psi = \hat{O}\psi(\boldsymbol{R}, \boldsymbol{r}), \tag{4}$$

with the operator

$$\hat{O} = \frac{1}{\sqrt{\hbar\hat{v}}} e^{i\hat{K}\cdot Z}, \tag{5}$$

where $\hat{K} = \sqrt{2\mu(E-h)}/\hbar$ and $\hat{v} = \hbar\hat{K}/\mu$ are wave-number and velocity operators of the motion of deuteron relative to T, respectively. When Eq. (4) is inserted into Eq. (3), we have a term including $\nabla_R^2\psi$, but it is neglected, since ψ is slowly varying with $\boldsymbol{R}$ compared with $\hat{O}$. The neglect leads Eq. (3) to

$$i\frac{d\psi}{dZ} = \hat{O}^\dagger U \hat{O}\psi. \tag{6}$$

Regarding Z as "time" and solving Eq. (6) iteratively, we obtain the formal solution

$$\psi = \exp\left[-i\mathcal{P}\int_{-\infty}^{Z} dZ'\hat{O}^\dagger U \hat{O}\right], \tag{7}$$

where $\mathcal{P}$ is the "time" ordering operator. Taking Z to ∞ in Eq. (7), we get the S-matrix operator

$$S = \exp\left[-i\mathcal{P}\int_{-\infty}^{\infty} dZ\hat{O}^\dagger U \hat{O}\right]. \tag{8}$$

In the Glauber model, h is replaced by the ground-state energy ϵ_0 of d. This adiabatic approximation reduces $\hat{O}^\dagger U \hat{O}$ and $\mathcal{P}$ in Eq. (8) to $U/(\hbar v_0)$ and 1, respectively, where v_0 is the velocity of d in the ground state relative to T. This is nothing but the S matrix in the Glauber model. Thus, ERT is an extension of the Glauber model.

The operator $\hat{O}^\dagger U \hat{O}$ describes the change in the motion of p and n in d during the collision. The change is small for the short-range nuclear interactions, $U_p^{(\mathrm{N})}$ and $U_n^{(\mathrm{N})}$, while large for the long-range Coulomb interaction $U_p^{(\mathrm{C})}$. Therefore, the adiabatic approximation that neglects this change is good for the nuclear interactions but not for the Coulomb interaction.

More quantitative discussion can be made by considering the matrix element

$$\int_{-\infty}^{\infty} dZ\langle\phi_{\boldsymbol{k}}|\hat{O}^\dagger U \hat{O}|\phi_0\rangle \approx \frac{e^{i(K_0-K)R_U}}{\hbar v_0}\int_{-\infty}^{\infty} dZ\langle\phi_{\boldsymbol{k}}|U|\phi_0\rangle \tag{9}$$

between the ground state ϕ_0 of d with the intrinsic energy ϵ_0 and its continuum state $\phi_{\boldsymbol{k}}$ with the intrinsic momentum $\hbar\boldsymbol{k}$ and energy ϵ, where $\hbar K_0$ ($\hbar K$) is the momentum of d in the ground (continuum) state relative to T, and R_U is the range of the interaction considered. As an example, let us consider the $d + {}^{208}$Pb scattering at 200 MeV/nucleon. The spectrum of the elastic breakup reaction, $d\sigma_{\mathrm{EB}}/d\epsilon$, has a peak around $\epsilon = 10$ MeV. The interaction range R_U is about 7.1 fm for the nuclear interactions, $U_p^{(\mathrm{N})}$ and $U_n^{(\mathrm{N})}$, while that for the Coulomb interaction $U_p^{(\mathrm{C})}$ is infinity. Hence, $\Delta = (K_0 - K)R_U \approx 0.55 < \pi$ for the nuclear interactions but ∞ for $U_p^{(\mathrm{C})}$. Since the adiabatic approximation is good for $\Delta \ll \pi$, the approximation is acceptable for the nuclear interactions but not for the Coulomb interaction. Actually, the breakup cross section is known to diverge in the adiabatic approximation [5,28].

The fact that the adiabatic approximation is fairly good for $U_n^{(\mathrm{N})}$ indicates that $U_n^{(\mathrm{N})}$ is commutable with $\hat{O}$. Therefore, we can make the replacement

$$\hat{O}^\dagger U_n^{(\mathrm{N})}\hat{O} \leftrightarrow U_n^{(\mathrm{N})}/(\hbar v_0). \tag{10}$$

The accuracy of Eq. (10) is confirmed later by numerical calculations. Using Eq. (10), we get

$$S = S_n S_p, \tag{11}$$

with

$$S_n = \exp\left[-i\mathcal{P}\int_{-\infty}^{\infty} dZ\, O^\dagger U_n^{(\mathrm{N})}\hat{O}\right], \tag{12}$$

$$S_p = \exp\left[-i\mathcal{P}\int_{-\infty}^{\infty} dZ\, \hat{O}^\dagger\left(U_p^{(\mathrm{N})}+U_p^{(\mathrm{C})}\right)\hat{O}\right]. \tag{13}$$

Thus, S can be separated into the neutron and proton parts, S_n and S_p, respectively. The neutron part S_n describes scattering of n by $U_n^{(\mathrm{N})}$ and recoil of p by the scattering. However, a velocity caused by the recoil is much smaller than the initial velocity v_0 of p, so that the recoil effect is negligible. Similar interpretation is possible for S_p. The operator S_p is the formal solution of the Schrödinger equation,

$$\left[-\frac{\hbar^2}{2\mu}\nabla_R^2 + h + U_p^{(\mathrm{N})}(r_p) + U_p^{(\mathrm{C})}(r_p) - E\right]\Psi_p = 0, \tag{14}$$

and S_n is the solution of the Schrödinger equation,

$$\left[-\frac{\hbar^2}{2\mu}\nabla_R^2 + h + U_n^{(\mathrm{N})}(r_n) - E\right]\Psi_n = 0. \tag{15}$$

Hence, the matrix elements of S_n and S_p can be obtained by solving Eqs. (14) and (15) with eikonal-CDCC [28], in which the eikonal approximation is made in CDCC calculations. Non-eikonal corrections to S_n and S_p can be easily made by using CDCC instead of eikonal-CDCC in solving Eqs. (14) and (15).

C. Integrated cross sections

In this subsection, we derive several formulas of integrated cross sections with the product form [Eq. (11)], following the formulation of the cross sections in the Glauber model [7,39]. The reaction and elastic-breakup cross sections, σ_{R} and σ_{EB}, respectively, are defined by

$$\sigma_{\mathrm{R}} = \int d^2\boldsymbol{b}[1 - |\langle\phi_0|S_pS_n|\phi_0\rangle|^2], \tag{16}$$

$$\sigma_{\mathrm{EB}} = \int d^2\boldsymbol{b}[\langle\phi_0||S_pS_n|^2|\phi_0\rangle - |\langle\phi_0|S_pS_n|\phi_0\rangle|^2]. \tag{17}$$

The cross sections σ_{R} and σ_{EB} can be evaluated from the asymptotic form of Ψ that is obtained by solving Eq. (3) with CDCC.

The total fusion cross section σ_{TF} is defined by

$$\sigma_{\mathrm{TF}} = \sigma_{\mathrm{R}} - \sigma_{\mathrm{EB}} = \int d^2\boldsymbol{b}\langle\phi_0|[(1 - |S_pS_n|^2)]|\phi_0\rangle. \tag{18}$$

The total fusion cross section can be decomposed into the neutron-stripping cross section $\sigma_{n:\mathrm{STR}}$, the proton-stripping cross section $\sigma_{p:\mathrm{STR}}$, and the complete-fusion cross section σ_{CF}:

$$\sigma_{\mathrm{TF}} = \sigma_{n:\mathrm{STR}} + \sigma_{p:\mathrm{STR}} + \sigma_{\mathrm{CF}}, \tag{19}$$

where

$$\sigma_{n:\mathrm{STR}} = \int d^2\boldsymbol{b}\langle\phi_0||S_p|^2(1 - |S_n|^2)|\phi_0\rangle, \tag{20}$$

$$\sigma_{p:\mathrm{STR}} = \int d^2\boldsymbol{b}\langle\phi_0||S_n|^2(1 - |S_p|^2)|\phi_0\rangle, \tag{21}$$

$$\sigma_{\mathrm{CF}} = \int d^2\boldsymbol{b}\langle\phi_0|(1 - |S_n|^2)(1 - |S_p|^2)|\phi_0\rangle. \tag{22}$$

The factor $|S_p|^2(1 - |S_n|^2)$ in $\sigma_{n:\mathrm{STR}}$ shows that p is scattered by T while n is absorbed by T, and the factor $(1 - |S_n|^2)(1 - |S_p|^2)$ in σ_{CF} means that both p and n are absorbed by T. The sum of $\sigma_{n:\mathrm{STR}}$ and $\sigma_{p:\mathrm{STR}}$ describes the incomplete fusion cross section σ_{IF}:

$$\sigma_{\mathrm{IF}} = \sigma_{n:\mathrm{STR}} + \sigma_{p:\mathrm{STR}}. \tag{23}$$

In the neutron removal reaction, n is either absorbed or scattered by T, while p is independently scattered by T. Hence, the cross section σ_{-n} is the sum of σ_{EB} and $\sigma_{n:\mathrm{STR}}$:

$$\sigma_{-n} = \sigma_{\mathrm{EB}} + \sigma_{n:\mathrm{STR}}. \tag{24}$$

The neutron-stripping cross section $\sigma_{n:\mathrm{STR}}$ is rewritten into

$$\begin{aligned}\sigma_{n:\mathrm{STR}} &= \int d^2\boldsymbol{b}\langle\phi_0|[(1 - |S_pS_n|^2) - (1 - |S_p|^2)]|\phi_0\rangle \\ &= \sigma_{\mathrm{TF}} - \sigma_{\mathrm{TF}}(p),\end{aligned} \tag{25}$$

where

$$\sigma_{\mathrm{TF}}(p) = \sigma_{\mathrm{R}}(p) - \sigma_{\mathrm{EB}}(p), \tag{26}$$

with

$$\sigma_{\mathrm{R}}(p) = \int d^2\boldsymbol{b}[1 - |\langle\phi_0|S_p|\phi_0\rangle|^2], \tag{27}$$

$$\sigma_{\mathrm{EB}}(p) = \int d^2\boldsymbol{b}[\langle\phi_0||S_p|^2|\phi_0\rangle - |\langle\phi_0|S_p|\phi_0\rangle|^2]. \tag{28}$$

Here, $\sigma_{\mathrm{TF}}(p)$, $\sigma_{\mathrm{R}}(p)$ and $\sigma_{\mathrm{EB}}(p)$ are the total fusion, reaction, and elastic-breakup cross sections induced by $U_p^{(\mathrm{N})} + U_p^{(\mathrm{C})}$ only. The cross sections, $\sigma_{\mathrm{R}}(p)$ and $\sigma_{\mathrm{EB}}(p)$, can be evaluated from the asymptotic form of Ψ_p that are obtained by solving Eq. (14) with CDCC. Thus, we can evaluate $\sigma_{n:\mathrm{STR}}$ with Eq. (25).

Similarly, the proton removal cross section σ_{-p} is obtained by

$$\sigma_{-p} = \sigma_{\mathrm{EB}} + \sigma_{p:\mathrm{STR}}, \tag{29}$$

and the proton-stripping cross section $\sigma_{p:\mathrm{STR}}$ is rewritten into

$$\sigma_{p:\mathrm{STR}} = \sigma_{\mathrm{TF}} - \sigma_{\mathrm{TF}}(n), \tag{30}$$

where

$$\sigma_{\mathrm{TF}}(n) = \sigma_{\mathrm{R}}(n) - \sigma_{\mathrm{EB}}(n), \tag{31}$$

with

$$\sigma_{\mathrm{R}}(n) = \int d^2\boldsymbol{b}[1 - |\langle\phi_0|S_n|\phi_0\rangle|^2], \tag{32}$$

$$\sigma_{\mathrm{EB}}(n) = \int d^2\boldsymbol{b}[\langle\phi_0||S_n|^2|\phi_0\rangle - |\langle\phi_0|S_n|\phi_0\rangle|^2]. \tag{33}$$

The cross sections, $\sigma_{\mathrm{R}}(n)$ and $\sigma_{\mathrm{EB}}(n)$, can be evaluated from the asymptotic form of Ψ_n that are obtained by solving

Eq. (15) with CDCC. We can thus evaluate $\sigma_{p:\mathrm{STR}}$ with Eq. (30). Finally, σ_{CF} is obtained from σ_{TF} and $\sigma_{\mathrm{IF}} = \sigma_{n:\mathrm{STR}} + \sigma_{p:\mathrm{STR}}$ by using the relation $\sigma_{\mathrm{CF}} = \sigma_{\mathrm{TF}} - \sigma_{\mathrm{IF}}$.

D. Tests of the eikonal and the adiabatic approximation

In ERT, non-eikonal corrections to the integrated cross sections are taken into account by using CDCC instead of eikonal-CDCC. For the $d + {}^{9}$Be scattering at 200 MeV/nucleon, the correction is found to be less than 1% for σ_{R}, σ_{EB}, $\sigma_{n:\mathrm{STR}}$, and $\sigma_{p:\mathrm{STR}}$. For the $d + {}^{208}$Pb scattering at 200 MeV/nucleon, the correction is 1.5% for σ_{R}, σ_{EB}, and $\sigma_{n:\mathrm{STR}}$ and 16% for $\sigma_{p:\mathrm{STR}}$. Thus, the non-eikonal correction is small except for $\sigma_{p:\mathrm{STR}}$ for heavy targets. As shown in Eq. (30), $\sigma_{p:\mathrm{STR}}$ is approximately obtained by

$$\sigma_{p:\mathrm{STR}} \approx \sigma_{\mathrm{R}} - \sigma_{\mathrm{R}}(n), \tag{34}$$

since $\sigma_{\mathrm{EB}} \ll \sigma_{\mathrm{R}}$. The 1.5% correction appears in σ_{R} because of the strong Coulomb field, while the correction is negligible in $\sigma_{\mathrm{R}}(n)$ as a consequence of the absence of the Coulomb field. Thus, one can conclude that the 16% correction required for $\sigma_{p:\mathrm{STR}}$ is nothing but the 1.5% correction for σ_{R}. Note that $\sigma_{p:\mathrm{STR}}$ is much smaller than σ_{R}. Meanwhile, $\sigma_{n:\mathrm{STR}}$ is given by

$$\sigma_{n:\mathrm{STR}} \approx \sigma_{\mathrm{R}} - \sigma_{\mathrm{R}}(p). \tag{35}$$

The 1.5% corrections appear in both σ_{R} and $\sigma_{\mathrm{R}}(p)$. The cancellation between the two corrections makes the non-eikonal correction small for $\sigma_{n:\mathrm{STR}}$.

In ERT, the adiabatic approximation is assumed to be good for the nuclear potential $U_n^{(\mathrm{N})}$. This can be tested by setting

$$U(R, r_n) = U_p^{(\mathrm{C})}(R) + U_p^{(\mathrm{N})}(R) + U_n^{(\mathrm{N})}(r_n)$$

in the Schrödinger equation [Eq. (3)]. In this setup, the projectile breakup is induced only by $U_n^{(\mathrm{N})}(r_n)$, since the argument r_p of $U_p^{(\mathrm{C})}$ and $U_p^{(\mathrm{N})}$ has been replaced by R. Switching the adiabatic approximation on the Schrödinger equation corresponds to the replacement [Eq. (10)]. For the $d + {}^{9}$Be scattering at 200 MeV/nucleon, the error due to the approximation is 0.3% for σ_{R} and 2% for σ_{EB}. For the $d + {}^{208}$Pb scattering at 200 MeV/nucleon, the error is 0.4% for σ_{R} and 6% for σ_{EB}. Errors due to these approximations are even smaller for heavier projectiles such as ^{31}Ne [38].

III. NUMERICAL RESULTS

We use the Koning-Delaroche global optical potential [40] as $U_p^{(\mathrm{N})}$ and $U_n^{(\mathrm{N})}$, and the Ohmura potential [41] as V that reproduces the deuteron-binding energy $|\varepsilon_0| = 2.23$ MeV. As the model space of CDCC calculation, s-, p-, and d-wave breakup states with $k \leqslant 1.0\ \mathrm{fm}^{-1}$ are taken. Each k continuum is divided into small bins with a common width $\Delta k = 0.1\ \mathrm{fm}^{-1}$, and the breakup states within each bin are averaged into a single state. Maximum values of r and R are $r_{\max} = 200$ fm and $R_{\max} = 200$ fm, respectively.

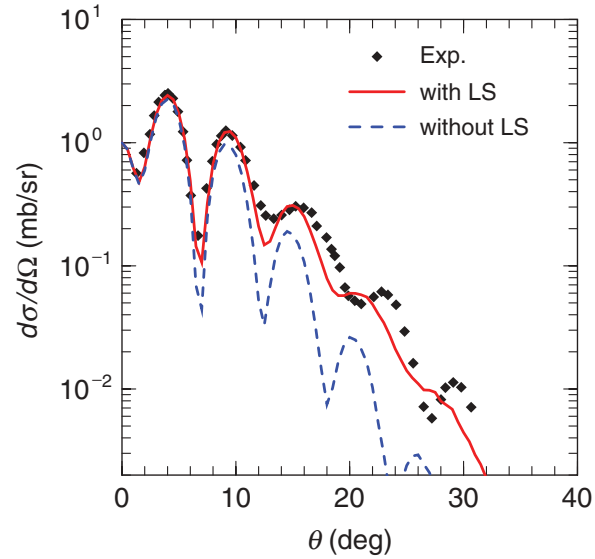

FIG. 1. (Color online) The elastic cross section of $d + {}^{58}$Ni scattering at 200 MeV/nucleon as a function of the c.m. scattering angle θ. The solid (dashed) line stands for result of CDCC calculation with (without) the spin-orbit interactions of the proton and neutron optical potentials. The experimental data are taken from Ref. [42].

A. $d + {}^{58}$Ni elastic scattering at 400 MeV

In this subsection, we consider the $d + {}^{58}$Ni elastic scattering at 200 MeV/nucleon, because the elastic cross section was measured and the reaction cross section was evaluated with the optical potential analysis [42].

Figure 1 shows the elastic cross section as a function of the center-of-mass (c.m.) scattering angle θ. The solid (dashed) line represents a result of CDCC calculation with (without) the spin-orbit interactions of $U_p^{(\mathrm{N})}$ and $U_n^{(\mathrm{N})}$. The solid line well reproduces the experimental data. Large deviation of the dashed line from the solid line for $\theta \gtrsim 10^\circ$ shows that the spin-orbit interactions yield a significant effect on the elastic cross section.

In the Glauber model, the spin-orbit interactions and the Coulomb breakup are neglected, and furthermore, the eikonal and the adiabatic approximation are made. The Coulomb breakup can be neglected by replacing $U_p^{(\mathrm{C})}(r_p)$ by $U_p^{(\mathrm{C})}(R)$ in CDCC calculation. In Fig. 2, the dotted line is the result of CDCC calculation, neglecting both the spin-orbit interactions and the Coulomb breakup. The dotted line agrees with the dashed line of Fig. 1, that is, the result of CDCC calculation with the Coulomb breakup and without spin-orbit interactions. Thus, the Coulomb-breakup effect is small. In Fig. 2, the dot-dashed line represents a result of the Glauber-model calculation. The large deviation of the dot-dashed line from the dotted line comes from the eikonal and adiabatic approximations, more precisely from the eikonal approximation. Eventually, the result of the Glauber model (the dot-dashed line) largely deviates from the full-CDCC result (the solid line) in which both the spin-orbit interactions and the Coulomb breakup are taken into account. Thus, the Glauber model does not work well for the elastic cross section for $\theta \gtrsim 10^\circ$.

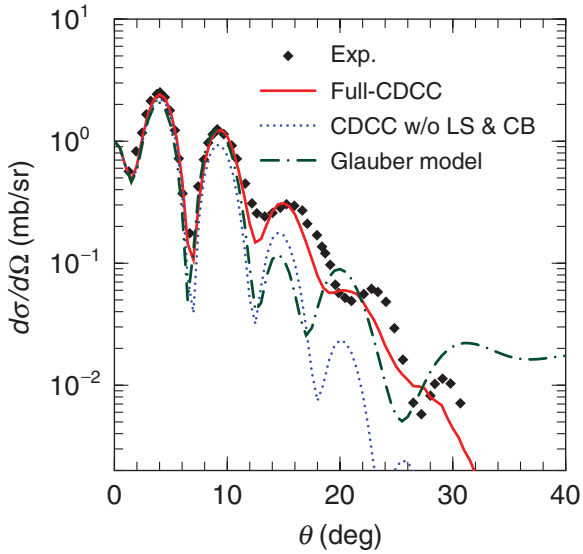

FIG. 2. (Color online) Comparison of the Glauber model with CDCC for the elastic cross section of $d+{}^{58}$Ni scattering at 200 MeV/nucleon. The solid line is the same as the solid line in Fig. 1. The dotted line stands for the result of CDCC calculation, neglecting both spin-orbit interactions and Coulomb breakup. The dot-dashed line represents the result of the Glauber-model calculation. The experimental data are taken from Ref. [42].

The reaction cross section calculated by full-CDCC is 1056 mb, while the value extracted from the measured elastic cross section with an optical model analysis is 1083 mb [42]. Thus, the CDCC result is consistent with the experimental data. Table I shows effects of the spin-orbit interactions and the Coulomb breakup on $\sigma_{\rm R}$, $\sigma_{\rm EB}$, and $\sigma_{\rm TF}$. Comparing the results with each other, one can find that the Coulomb breakup effect is about 50% for $\sigma_{\rm EB}$ and 2% for $\sigma_{\rm R}$, while the spin-orbit interaction effect is 17% for $\sigma_{\rm EB}$ and 1% for $\sigma_{\rm R}$. Thus, the effects are sizable for $\sigma_{\rm EB}$ and appreciable for $\sigma_{\rm R}$. Meanwhile, these effects are quite small for $\sigma_{\rm TF}$, because the absolute value of S is mainly determined by the imaginary parts of $U_n^{\rm (N)}$ and $U_p^{\rm (N)}$. This is also the case with $\sigma_{p:\rm STR}$, $\sigma_{n:\rm STR}$, $\sigma_{\rm IF}$, and $\sigma_{\rm CF}$. Table I shows that the spin-orbit interaction effect is even smaller than the Coulomb-breakup effect. We henceforth neglect the spin-orbit interactions but not the Coulomb breakup, since the Coulomb breakup becomes more significant for heavier targets.

TABLE I. Effects of the spin-orbit interaction and the Coulomb breakup on $\sigma_{\rm R}$, $\sigma_{\rm EB}$, and $\sigma_{\rm TF}$ for the $d+{}^{58}$Ni scattering at 200 MeV/nucleon. The experimental data is taken from Ref. [42]. The cross sections are shown in units of mb.

	Coulomb breakup	spin-orbit	$\sigma_{\rm R}$	$\sigma_{\rm EB}$	$\sigma_{\rm TF}$
CDCC	on	on	1056	59	997
	on	off	1066	69	997
	off	on	1029	31	998
	off	off	1023	25	998
Exp.			1083		

B. Inclusive ^{7}Li(d,n) reaction at 40 MeV

The double-differential cross section (DDX) of inclusive ^{7}Li(d,n) reaction was measured at 40 MeV [17]. The main part of the DDX consists of the elastic-breakup and the proton-stripping parts. When the elastic-breakup DDX is calculated with CDCC and subtracted from the measured DDX, the angular and the energy dependence of the remaining DDX is well reproduced by the Glauber model [18]. This indicates that the proton-stripping cross section $\sigma_{p:\rm STR}$ can be obtained by fitting the theoretical DDX calculated by the Glauber model to the remaining DDX and integrating it over the angle and the energy. The $\sigma_{p:\rm STR}$ thus extracted is 244 ± 34(theor.) $\pm$ 37(exp.) mb; the theoretical error comes from ambiguity of the fitting. ERT gives $\sigma_{p:\rm STR} = 253$ mb and the Glauber model does 214 mb. Thus, the two theoretical results are consistent with the experimental data. The ERT result seems to be slightly better than the Glauber-model result for this case.

C. Relation between reaction and elastic-breakup cross sections

In this subsection, we discuss the relation between $\sigma_{\rm R}$ and $\sigma_{\rm EB}$ for deuteron-induced reactions at 200 MeV/nucleon.

In the framework of CDCC, $\sigma_{\rm R}$ is the sum of the partial reaction cross section $\sigma_{\rm R}(J)$ over the total angular momentum J, while $\sigma_{\rm EB}$ is the sum of the partial-breakup cross sections $\sigma_{\rm EB}(J)$:

$$\sigma_{\rm R} = \sum_J \sigma_{\rm R}(J) = \frac{\pi}{K_0^2}\sum_J (2J+1)P_{\rm R}(J), \tag{36}$$

$$\sigma_{\rm EB} = \sum_J \sigma_{\rm EB}(J) = \frac{\pi}{K_0^2}\sum_J (2J+1)P_{\rm EB}(J), \tag{37}$$

with

$$P_{\rm R}(J) = 1 - |\langle 0|S(J)|0\rangle|^2, \tag{38}$$

$$P_{\rm EB}(J) = \sum_\beta |\langle \beta|S(J)|0\rangle|^2, \tag{39}$$

where K_0 is the initial wave number of d. The partial elastic and breakup S-matrix elements are denoted by $\langle 0|S(J)|0\rangle$ and $\langle \beta|S(J)|0\rangle$, respectively, where 0 (β) represents the elastic (breakup) channel. The quantity $P_{\rm R}(J)$ shows, for each J, the transition probability of the incident flux to all channels except the elastic channel, while $P_{\rm EB}(J)$ describes the transition probability to all the breakup channels. The probability $P_{\rm EB}(J)$ can be rewritten into

$$P_{\rm EB}(J) = \langle 0|S(J)^\dagger S(J)|0\rangle - |\langle 0|S(J)|0\rangle|^2. \tag{40}$$

This indicates that $P_{\rm EB}(J)$ is the fluctuation of the mean value $|\langle 0|S(J)|0\rangle|$ for each J. In general, a rapid change in $|\langle 0|S(J)|0\rangle|$, with respect to J, occurs where the fluctuation becomes maximum. Since $P_{\rm R}(J)$ is a function of $|\langle 0|S(J)|0\rangle|$, one can expect that $P_{\rm R}(J)$ is rapidly changed where $P_{\rm EB}(J)$ becomes maximum. We return to this point below.

The transition probabilities $P_{\rm R}$ and $P_{\rm EB}$ are plotted in Fig. 3 as a function of the effective distance $R \equiv (J+1/2)/K_0$ between the projectile and the target. For heavier targets, ^{58}Ni, ^{93}Nb, and ^{208}Pb, $P_{\rm R}$ behaves as a logistic function and

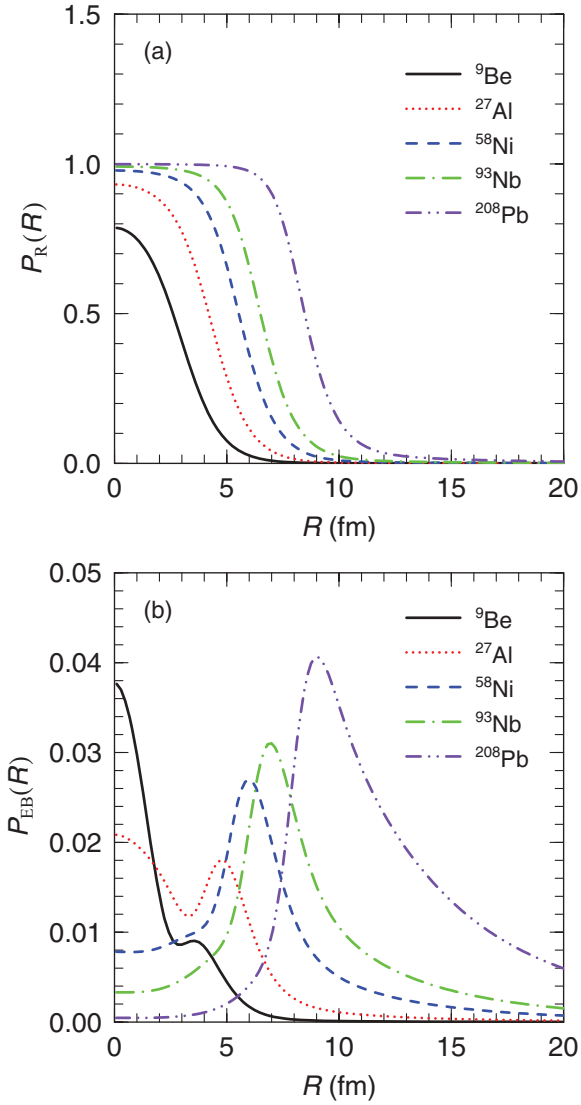

FIG. 3. (Color online) Transition probabilities P_R and P_{EB} as a function of $R = (J + 1/2)/K_0$ for deuteron scattering at 200 MeV/nucleon.

hence the R dependence is close to a step function. This indicates that the reaction cross section can be approximately described by the black-sphere model [43]. Therefore, σ_R can be expressed by the area of a disk,

$$\sigma_R = \pi R_R^2, \tag{41}$$

with effective radius R_R. Meanwhile, the elastic-breakup reaction is peripheral, since P_{EB} has a single peak at a finite value of R. An effective radius R_{EB} of σ_{EB} can be defined by the peak of P_{EB}. As expected, P_R changes rapidly at $R = R_{EB}$. This indicates that

$$R_R = R_{EB}. \tag{42}$$

For lighter targets such as ^{9}Be and ^{27}Al, P_{EB} has two peaks; the first peak is located at $R = 0$ and the second at finite value of R. However, the second peak is more significant than the first peak in σ_R because of the weight factor of $2J + 1$ in Eq. (36). We thus define R_{EB} by the second peak.

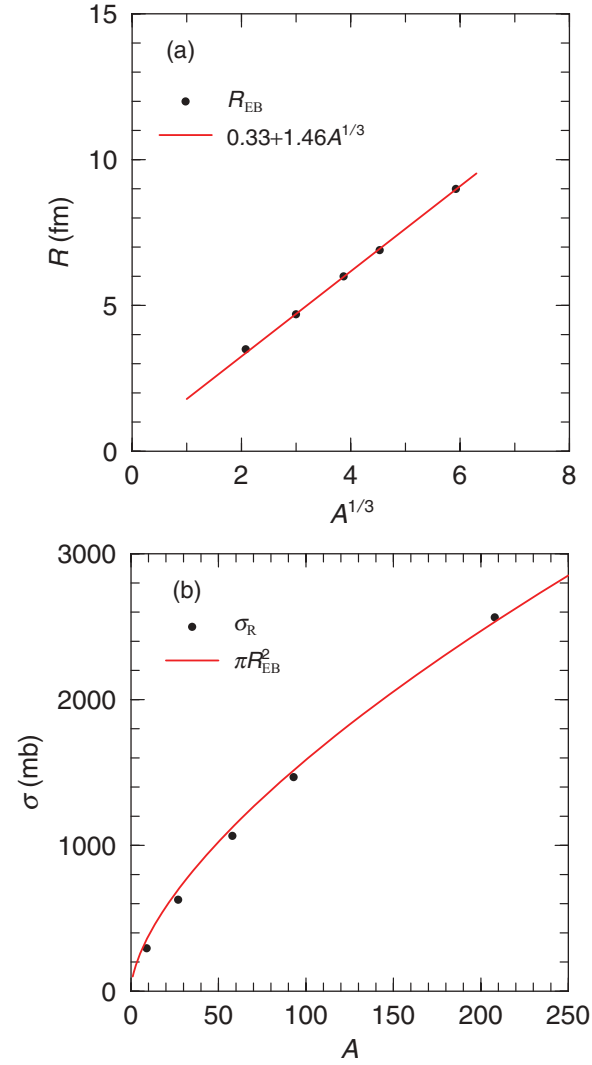

FIG. 4. (Color online) A dependence of (a) R_{EB} and (b) σ_R.

Figure 4(a) shows R_{EB} as a function of $A^{1/3}$, where A is the target mass number. Since the elastic-breakup reaction is peripheral, R_{EB} is expected to depend on $A^{1/3}$. Actually, A-dependence of R_{EB} is well fitted by a straight line (the solid line)

$$R_{EB} = 0.33 + 1.46A^{1/3}. \tag{43}$$

The fitting is made only for heavier targets of ^{58}Ni, ^{93}Nb, and ^{208}Pb, where $P_{EB}(J)$ has a single peak. Figure 4(b) shows A-dependence of σ_R, where the solid curve is obtained from Eq. (41) with Eqs. (42) and (43), while closed circles stand for the results of CDCC. Both results agree with each other. Thus, the formula (42) is well satisfied.

D. A-dependence of integrated cross sections

A-dependence of integrated cross sections is discussed for deuteron-induced reactions at 200 MeV/nucleon. Integrated cross sections calculated by CDCC and ERT are tabulated in Table II.

TABLE II. Integrated cross sections calculated with CDCC and ERT. The cross sections are shown in units of mb.

Nuclide	σ_R	σ_{EB}	σ_{TF}	$\sigma_{n:STR}$	σ_{-n}	$\sigma_{p:STR}$	σ_{-p}	σ_{CF}
^{9}Be	295	11	284	111	122	133	144	40
^{27}Al	628	30	598	211	241	245	275	144
^{58}Ni	1066	69	997	312	381	343	412	342
^{93}Nb	1469	110	1359	387	497	406	516	566
^{208}Pb	2565	275	2290	540	815	489	764	1261

First, we consider the total-fusion cross section σ_{TF}. The cross section is obtained by subtracting the area of the ring $\sigma_{EB}(J)$ from that of the disk $\sigma_R(J)$. Thus, it can be described also by the area of a disk,

$$\sigma_{TF} = \pi R_{TF}^2, \tag{44}$$

with effective radius R_{TF}. Similar definition is possible for $\sigma_{TF}(p)$ and $\sigma_{TF}(n)$:

$$\sigma_{TF}(p) = \pi R_{TF}(p)^2, \sigma_{TF}(n) = \pi R_{TF}(n)^2. \tag{45}$$

Figure 5 presents R_{TF}, $R_{TF}(p)$, and $R_{TF}(n)$ as a function of $A^{1/3}$. Symbols show effective radii evaluated from the CDCC total-fusion cross sections in Table II. They can be fitted by straight lines:

$$R_{TF} = 0.18 + 1.41A^{1/3}, \tag{46}$$
$$R_{TF}(p) = -0.60 + 1.36A^{1/3}, \tag{47}$$
$$R_{TF}(n) = -1.09 + 1.46A^{1/3}. \tag{48}$$

This fitting is made only for heavier targets, ^{58}Ni, ^{93}Nb, and ^{208}Pb, where $P_R(J)$ has a logistic shape, but the fitting is still good for lighter targets of ^{9}Be and ^{27}Al.

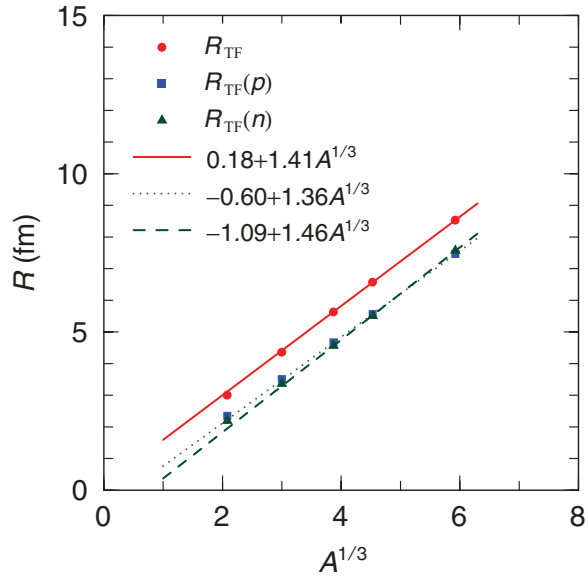

FIG. 5. (Color online) A-dependence of R_{TF}, $R_{TF}(p)$, and $R_{TF}(n)$. The symbols denote the results of CDCC, while the lines stand for the results of the straight-line fitting.

The neutron-stripping cross section is obtained from R_{TF} and $R_{TF}(p)$ as

$$\sigma_{n:STR} = \pi\left[R_{TF}^2 - R_{TF}(p)^2\right] = 2\pi D_{n:STR} R_{n:STR}, \tag{49}$$

with

$$D_{n:STR} = R_{TF} - R_{TF}(p), \tag{50}$$
$$R_{n:STR} = [R_{TF} + R_{TF}(p)]/2. \tag{51}$$

Thus, the neutron-stripping reaction occurs on a ring of effective radius $R_{n:STR}$ and effective width $D_{n:STR}$. The effective width $D_{n:STR}$ has small A-dependence because of the cancellation between R_{TF} and $R_{TF}(p)$. Similar discussion can be made for the proton-stripping cross section:

$$\sigma_{p:STR} = 2\pi D_{p:STR} R_{p:STR}, \tag{52}$$

with

$$D_{p:STR} = R_{TF} - R_{TF}(n), \tag{53}$$
$$R_{p:STR} = [R_{TF} + R_{TF}(n)]/2. \tag{54}$$

The effective radii, $R_{n:STR}$ and $R_{p:STR}$, and the effective widths, $D_{n:STR}$ and $D_{p:STR}$, are simply obtained from R_{TF}, $R_{TF}(p)$, and $R_{TF}(n)$:

$$R_{n:STR} = -0.21 + 1.39A^{1/3}, \tag{55}$$
$$R_{p:STR} = -0.46 + 1.44A^{1/3}, \tag{56}$$
$$D_{n:STR} = 0.78 + 0.05A^{1/3}, \tag{57}$$
$$D_{p:STR} = 1.27 - 0.05A^{1/3}. \tag{58}$$

These are shown in Fig. 6 as a function of $A^{1/3}$. As expected, $D_{n:STR}$ and $D_{p:STR}$ have weak A-dependence. The values are about 1 fm corresponding to the diffuseness of the target density. Meanwhile, $R_{n:STR}$ and $R_{p:STR}$ has almost the same A-dependence as R_R.

The elastic-breakup reaction is peripheral as the stripping reactions. It is thus natural to assume that it occurs on a ring

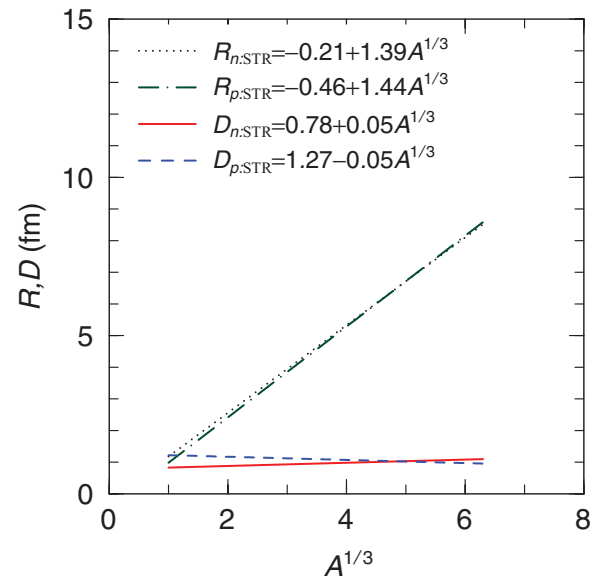

FIG. 6. (Color online) A dependence of $R_{n:STR}$, $R_{p:STR}$, $D_{n:STR}$, and $D_{p:STR}$.

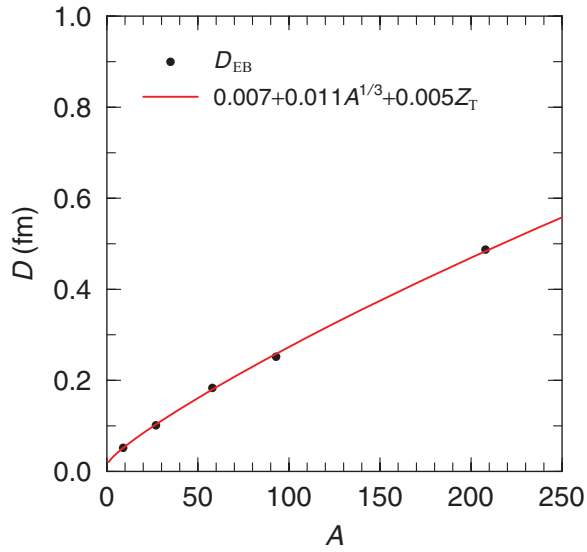

FIG. 7. (Color online) A dependence of D_{EB}.

with effective radius R_{EB} and effective width D_{EB}:

$$\sigma_{EB} = 2\pi D_{EB} R_{EB}. \tag{59}$$

The effective width D_{EB} may be parameterized by

$$D_{EB} = a + bA^{1/3} + cZ_T, \tag{60}$$

with parameters a, b, and c. Note that the role of Coulomb breakup, which is essential for σ_{EB}, is described by the last term cZ_T, where Z_T is the proton number of target. We use the relation between Z_T and A for nuclei on stability line,

$$Z_T = \frac{A}{2 + (a_C/a_A)A^{2/3}} = \frac{A}{2 + 0.015A^{2/3}}, \tag{61}$$

obtained from the Bethe-Weisäcker mass formula [44] neglecting pairing energy term, where $a_C = 0.697$ MeV and $a_A = 46.58$ MeV are coefficients of the Coulomb and asymmetry energy terms, respectively. The parametrization [Eq. (60)] indeed works well as shown in Fig. 7. The circles denote D_{EB} evaluated from the CDCC elastic-breakup cross section with Eq. (59). A-dependence of the CDCC results is well simulated by the solid line

$$D_{EB} = 0.007 + 0.011A^{1/3} + 0.005Z_T. \tag{62}$$

The D_{EB} is found to be smaller than $D_{n:STR}$ and $D_{p:STR}$.

It should be noted that the ring specified by R_{EB} and D_{EB} means the effective region of the elastic breakup process that corresponds to $P_{EB}(J) = 1$. Since the $P_{EB}(J)$ shown in the lower panel of Fig. 3 are significantly smaller than unity, the "actual" reaction region for elastic breakup has much wider width than in Fig. 7. Furthermore, for heavier targets, $P_{EB}(J)$ has a long-range tail, as a function of R, due to Coulomb breakup, which makes the actual reaction region even wider. Nevertheless, the use of Eq. (59) will be helpful for plain

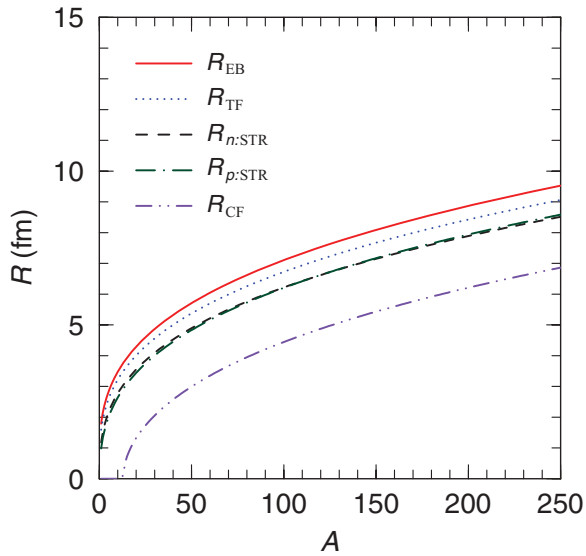

FIG. 8. (Color online) A dependence of R_{EB}, R_{TF}, $R_{n:STR}$, $R_{p:STR}$, and R_{CF}.

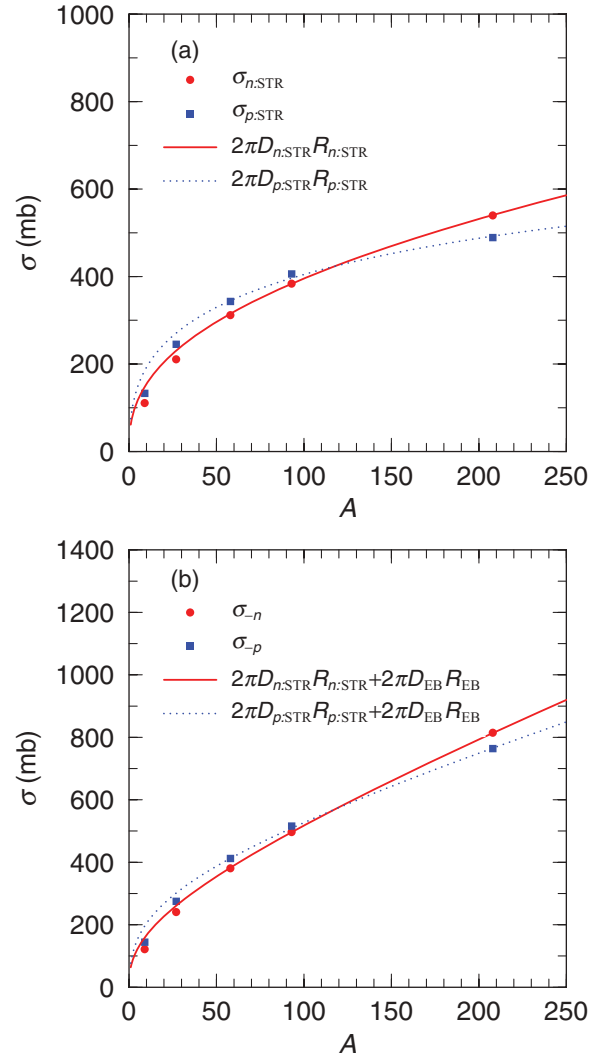

FIG. 9. (Color online) A-dependence of the stripping and removal cross sections. $\sigma_{n:STR}$ and $\sigma_{p:STR}$ are plotted in the upper panel, while σ_{-n} and σ_{-p} are shown in the lower panel. Symbols stand for results of CDCC and ERT. Lines denote results of the parametrization [Eqs. (49)–(66)].

understanding of the "effective" reaction region of elastic breakup.

Other integrated cross sections can be obtained by the combination of $\sigma_{\rm EB}$, $\sigma_{n:\rm STR}$, $\sigma_{p:\rm STR}$, and $\sigma_{\rm TF}$:

$$\sigma_{-n} = 2\pi D_{\rm EB} R_{\rm EB} + 2\pi D_{n:\rm STR} R_{n:\rm STR}, \quad (63)$$

$$\sigma_{-p} = 2\pi D_{\rm EB} R_{\rm EB} + 2\pi D_{p:\rm STR} R_{p:\rm STR}, \quad (64)$$

$$\sigma_{\rm IF} = 2\pi D_{n:\rm STR} R_{n:\rm STR} + 2\pi D_{p:\rm STR} R_{p:\rm STR}, \quad (65)$$

$$\sigma_{\rm CF} = \pi R_{\rm TF}^2 - \sigma_{\rm IF}. \quad (66)$$

One can thus define effective radii $R_{\rm CF}$ of the complete fusion cross sections by

$$\sigma_{\rm CF} \equiv \pi R_{\rm CF}^2 \quad (67)$$

and can evaluate the value of $R_{\rm CF}$ from Eq. (66). A-dependence of $R_{\rm TF}$, $R_{n:\rm STR}$, $R_{p:\rm STR}$, $R_{\rm EB}$, and $R_{\rm CF}$ is summarized in Fig. 8. The order of the effective radii is $R_{\rm CF} < R_{p:\rm STR} \approx R_{n:\rm STR} < R_{\rm TF} < R_{\rm R} = R_{\rm EB}$, independently of A. Among these reactions, the elastic-breakup reaction is most peripheral, and it occurs at $R_{\rm EB} - D_{\rm EB}/2 \lesssim R \lesssim R_{\rm EB} + D_{\rm EB}/2$. The incomplete fusion reactions take place at $R_{n:\rm STR} - D_{n:\rm STR}/2 \lesssim R \lesssim R_{n:\rm STR} + D_{n:\rm STR}/2$. At $R \lesssim R_{\rm CR}$, only the complete fusion reaction occurs.

The cross sections $\sigma_{n:\rm STR}$, $\sigma_{p:\rm STR}$, σ_{-n}, and σ_{-p} are plotted as a function of A in Fig. 9. The cross section $\sigma_{n:\rm STR}$ (σ_{-n}) has similar A-dependence to $\sigma_{p:\rm STR}$ (σ_{-p}). The removal cross sections have stronger A-dependence than the stripping cross sections, since the former include the elastic-breakup cross section.

A-dependence of $\sigma_{\rm R}$, $\sigma_{\rm TF}$, $\sigma_{\rm IF}$, and $\sigma_{\rm CF}$ is summarized in Fig. 10. For $A \lesssim 150$, $\sigma_{\rm IF}$ is larger than $\sigma_{\rm CF}$ and becomes the largest component of $\sigma_{\rm R}$, while for $A \lesssim 150$, $\sigma_{\rm CF}$ becomes the largest.

E. Accuracy of the Glauber model for integrated cross sections

The accuracy of the Glauber model is investigated for deuteron-induced reactions at 200 MeV/nucleon. For this purpose, we define the relative error

$$\delta_X = [X(\rm CDCC) - X(\rm GL)]/X(\rm CDCC), \quad (68)$$

where X(CDCC) and X(GL) are integrated cross sections calculated with CDCC and the Glauber model, respectively. In the Glauber-model calculation, the eikonal and adiabatic approximations are made and the Coulomb interaction is set to zero.

Figure 11 shows δ_X as a function of A for $\sigma_{\rm EB}$, σ_{-n}, and σ_{-p} in the upper panel and for $\sigma_{\rm R}$, $\sigma_{\rm TF}$, $\sigma_{n:\rm STR}$, $\sigma_{p:\rm STR}$, and $\sigma_{\rm CF}$ in the lower panel. For light targets, say ^{9}Be, the error is less than 2% for all integrated cross sections except $\sigma_{\rm CF}$. The error is 8% for $\sigma_{\rm CF}$, but $\sigma_{\rm CF}$ itself is small there. Thus, the Glauber model is good at small A, as expected.

For heavier targets, say ^{208}Pb, where the Coulomb breakup is essential, the error is 80% for $\sigma_{\rm EB}$, 20% for σ_{-n} and σ_{-p}, and −20% for $\sigma_{p:\rm STR}$. The error is slightly smaller for σ_{-p} than for σ_{-n}. However, this is just a result of the cancellation in σ_{-p} between the positive error for $\sigma_{\rm EB}$ and the negative error for

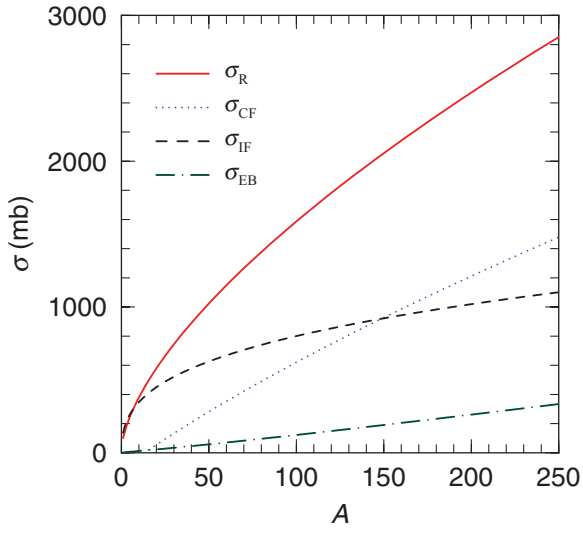

FIG. 10. (Color online) A-dependence of integrated cross sections.

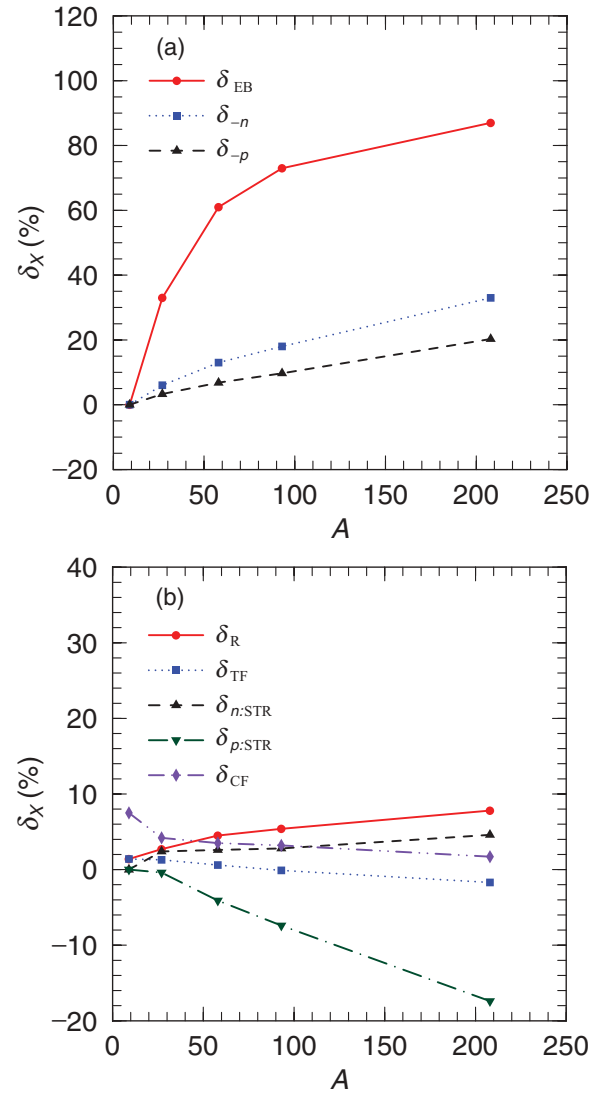

FIG. 11. (Color online) Accuracy of the Glauber model for integrated cross sections.

$\sigma_{p:\mathrm{STR}}$. The error is less than 6% for $\sigma_{n:\mathrm{STR}}$, σ_{R}, σ_{TF}, and σ_{CF}. Thus, the Glauber model is not good for σ_{EB}, σ_{-n}, and σ_{-p}.

IV. SUMMARY

The continuum-discretized coupled-channels method (CDCC) and the eikonal reaction theory (ERT) are applied to $d+{}^{58}$Ni elastic scattering at 200 MeV/nucleon and inclusive ^{7}Li(d,n) reaction at 40 MeV. For σ_{R} of the $d+{}^{58}$Ni scattering, the CDCC result is consistent with the experimental data. The spin-orbit interactions of the proton and neutron optical potentials yield a significant effect on the differential elastic-scattering cross section, but not on σ_{R}. For $\sigma_{p:\mathrm{STR}}$ of the $d+{}^{7}$Li scattering, the ERT result is consistent with the experimental data.

A-dependence of several types of integrated cross sections is systematically investigated with CDCC and ERT for the deuteron-induced reactions at 200 MeV/nucleon that corresponds to typical RIBF and GSI beam energies. The A-dependence is clearly explained with simple formulas as follows. A black-sphere-type reaction such as the reaction, total-fusion, and complete-fusion processes occurs on a disk with the area of πR_{X}^2 with effective radius R_{X} that is well parameterized by $a_{\mathrm{X}}+b_{\mathrm{X}}A^{1/3}$. A peripheral reaction such as the elastic-breakup, nucleon-stripping, and nucleon-removal processes takes place on a ring $2\pi D_{\mathrm{X}}R_{\mathrm{X}}$ with effective radius and width, R_{X} and D_{X}, and A-dependence of R_{X} is well parameterized by $a_{\mathrm{X}}+b_{\mathrm{X}}A^{1/3}$. For neutron- and proton-stripping reactions as the incomplete-fusion reaction, the effective widths, $D_{n:\mathrm{STR}}$ and $D_{p:\mathrm{STR}}$, are about 1 fm independently of A. The effective radii, $R_{n:\mathrm{STR}}$ and $R_{p:\mathrm{STR}}$, are smaller than effective radius R_{R} for the reaction cross section by about 1 fm independently of A, while effective radius R_{CF} for the complete-fusion cross section is smaller than R_{R} by about 2.5 fm independently of A. Thus, A-dependencies of R_{R}, $R_{n:\mathrm{STR}}$, $R_{p:\mathrm{STR}}$, and R_{CF} are simple and similar to each other. Thus, if σ_{R}, σ_{CF}, $\sigma_{n:\mathrm{STR}}$, and $\sigma_{p:\mathrm{STR}}$ are determined experimentally just for two targets, one can estimate these cross sections for any target. It is of interest as a future work to see whether this property is held for other incident energies and projectiles.

The total-fusion cross section σ_{TF} is obtained from measurable cross sections, σ_{R} and σ_{EB}, by $\sigma_{\mathrm{TF}}=\sigma_{\mathrm{R}}-\sigma_{\mathrm{EB}}$. Similarly, neutron- and proton-stripping cross sections are determined from measurable neutron- and proton-removal cross sections by $\sigma_{n:\mathrm{STR}}=\sigma_{-n}-\sigma_{\mathrm{EB}}$ and $\sigma_{p:\mathrm{STR}}=\sigma_{-p}-\sigma_{\mathrm{EB}}$. It is thus important to determine A-dependence of σ_{EB}. However, the A-dependence is known to be complicated [45,46], since it depends on not only A but also the target proton number Z_{T}. This problem can be solved by the formula $\sigma_{\mathrm{EB}}=2\pi D_{\mathrm{EB}}R_{\mathrm{EB}}$. Effective radius R_{EB} agrees with $R_{\mathrm{R}}=a_{\mathrm{R}}+b_{\mathrm{R}}A^{1/3}$ with high accuracy, and effective width D_{EB} is well parameterized by $a_{\mathrm{EB}}+b_{\mathrm{EB}}A^{1/3}+c_{\mathrm{EB}}Z_{\mathrm{T}}$. Thus, A-dependence of σ_{EB} is determined, if σ_{EB} is measured for three targets and σ_{R} is measured for two targets.

Accuracy of the Glauber model is also tested for the deuteron scattering at 200 MeV/nucleon. The accuracy for integrated cross sections is summarized as follows. The Glauber model is good for light targets, if the interactions between projectile and target are clearly determined. For heavy targets, however, the model is not good for the elastic-breakup, the nucleon-removal, and the proton-stripping cross sections, because of the strong Coulomb field, while it is fairly good for the other cross sections. It is quite interesting as a future work that similar systematic analyses will be made for heavier projectiles such as Ne and Ca isotopes with larger proton numbers. Energy-dependence of the various cross sections and corresponding effective radii and widths will also be an important subject.

ACKNOWLEDGMENTS

We are grateful to Y. Suzuki for useful discussions. We also acknowledge K. Hagino for valuable suggestions. S.H. would like to thank A. Kohama for helpful comments and discussions.

[1] A. Gade *et al.*, Phys. Rev. C **77**, 044306 (2008).
[2] H. Matsui, *Proceedings of the 23rd Symposium on Fusion Technology* (Venice, Italy, 2004).
[3] R. J. Glauber, in *Lectures in Theoretical Physics*, Vol. 1 (Interscience, New York, 1959), p. 315.
[4] M. Yahiro, K. Minomo, K. Ogata, and M. Kawai, Prog. Theor. Phys. **120**, 767 (2008).
[5] P. Capel, D. Baye, and Y. Suzuki, Phys. Rev. C **78**, 054602 (2008).
[6] J. S. Al Khalili and J. A. Tostevin, Phys. Rev. Lett. **76**, 3903 (1996); J. S. Al Khalili, J. A. Tostevin, and I. J. Thompson, Phys. Rev. C **54**, 1843 (1996).
[7] K. Hencken, G. Bertsch, and H. Esbensen, Phys. Rev. C **54**, 3043 (1996).
[8] K. Yabana, Y. Ogawa, and Y. Suzuki, Nucl. Phys. A **539**, 295 (1992).
[9] Y. Ogawa, K. Yabana, and Y. Suzuki, Nucl. Phys. A **543**, 722 (1992).
[10] Y. Ogawa, T. Kido, K. Yabana, and Y. Suzuki, Prog. Theor. Phys. Suppl. **142**, 157 (2001), and references cited therein.
[11] B. Abu Ibrahim and Y. Suzuki, Prog. Theor. Phys. **112**, 1013 (2004); *ibid.* **114**, 901 (2005).
[12] W. Horiuchi, Y. Suzuki, P. Capel, and D. Baye, Phys. Rev. C **81**, 024606 (2010).
[13] C. A. Bertulani and M. S. Hussein, Phys. Rev. Lett. **64**, 1099 (1990); Nucl. Phys. A **524**, 306 (1991).
[14] C. A. Bertulani and K. W. McVoy, Phys. Rev. C **46**, 2638(1992).
[15] T. Aumann, C. A. Bertulani, and K. Suemmerer, Phys. Rev. C **51**, 416 (1995).
[16] C. A. Bertulani and P. G. Hansen, Phys. Rev. C **70**, 034609 (2004).
[17] M. Hagiwara, T. Itoga, N. Kawata, N. Hirabayashi, T. Oishi, T. Yamauchi, M. Baba, M. Sugimoto, and T. Muroga, Fusion Sci. Technol. **48**, 1320 (2005).
[18] T. Ye, Y. Watanabe, and K. Ogata, Phys. Rev. C **80**, 014604 (2009).

[19] M. Kamimura, M. Yahiro, Y. Iseri, Y. Sakuragi, H. Kameyama, and M. Kawai, Prog. Theor. Phys. Suppl. **89**, 1 (1986).
[20] N. Austern, Y. Iseri, M. Kamimura, M. Kawai, G. Rawitscher, and M. Yahiro, Phys. Rep. **154**, 125 (1987).
[21] N. Austern, M. Yahiro, and M. Kawai, Phys. Rev. Lett. **63**, 2649 (1989).
[22] N. Austern, M. Kawai, and M. Yahiro, Phys. Rev. C **53**, 314 (1996).
[23] A. Deltuva, A. M. Moro, E. Cravo, F. M. Nunes, and A. C. Fonseca, Phys. Rev. C **76**, 064602 (2007).
[24] K. Rusek and K. W. Kemper, Phys. Rev. C **61**, 034608 (2000).
[25] J. A. Tostevin, F. M. Nunes, and I. J. Thompson, Phys. Rev. C **63**, 024617 (2001).
[26] B. Davids, S. M. Austin, D. Bazin, H. Esbensen, B. M. Sherrill, I. J. Thompson, and J. A. Tostevin, Phys. Rev. C **63**, 065806 (2001).
[27] J. Mortimer, I. J. Thompson, and J. A. Tostevin, Phys. Rev. C **65**, 064619 (2002).
[28] K. Ogata, M. Yahiro, Y. Iseri, T. Matsumoto, and M. Kamimura, Phys. Rev. C **68**, 064609 (2003).
[29] T. Matsumoto, E. Hiyama, K. Ogata, Y. Iseri, M. Kamimura, S. Chiba, and M. Yahiro, Phys. Rev. C **70**, 061601(R) (2004).
[30] D. J. Howell, J. A. Tostevin, and J. S. Al Khalili, J. Phys. G **31**, S1881 (2005).
[31] K. Rusek, I. Martel, J. Gómez-Camacho, A. M. Moro, and R. Raabe, Phys. Rev. C **72**, 037603 (2005).
[32] T. Matsumoto, T. Egami, K. Ogata, Y. Iseri, M. Kamimura, and M. Yahiro, Phys. Rev. C **73**, 051602(R) (2006).
[33] A. M. Moro, K. Rusek, J. M. Arias, J. Gómez-Camacho, and M. Rodríguez-Gallardo, Phys. Rev. C **75**, 064607 (2007).
[34] M. Rodríguez-Gallardo, J. M. Arias, J. Gómez-Camacho, R. C. Johnson, A. M. Moro, I. J. Thompson, and J. A. Tostevin, Phys. Rev. C **77**, 064609 (2008).
[35] M. Rodríguez-Gallardo, J. M. Arias, J. Gómez-Camacho, A. M. Moro, I. J. Thompson, and J. A. Tostevin, Phys. Rev. C **80**, 051601(R) (2009).
[36] T. Matsumoto, K. Kato, and M. Yahiro, Phys. Rev. C **82**, 051602 (2010).
[37] M. Avrigeanu and A. M. Moro, Phys. Rev. C **82**, 037601 (2010).
[38] M. Yahiro, K. Ogata, and K. Minomo, arXiv:1103.3976 [nucl-th] (2011).
[39] M. S. Hussein and K. W. McVoy, Nucl. Phys. A **445**, 124 (1985).
[40] A. J. Koning and J. P. Delaroche, Nucl. Phys. A **713**, 231 (2003).
[41] T. Ohmura, B. Imanishi, M. Ichimura, and M. Kawai, Prog. Theor. Phys. **43**, 347 (1970).
[42] N. van Sen *et al.*, Phys. Lett. B **156**, 185 (1985).
[43] A. Kohama, K. Iida, and K. Oyamatsu, Phys. Rev. C **72**, 024602 (2005).
[44] C. F. von Weizsäcker, Z. Phys. **96**, 431 (1935); H. A. Bethe and R. F. Bacher, Rev. Mod. Phys. **8**, 82 (1936).
[45] M. S. Hussein, R. Lichtenthäler, F. M. Nunes, and I. J. Thompson, Phys. Lett. B **640**, 91 (2006).
[46] K. Ogata, T. Matsumoto, Y. Iseri, and M. Yahiro, J. Phys. Soc. Jap. **78**, 084201 (2009).